

# Octupole states in deformed actinide nuclei with the interacting boson approximation

P. D. Cottle

*Department of Physics, Florida State University, Tallahassee, Florida 32306-4350*

N. V. Zamfir

*WNSL, Yale University, New Haven, Connecticut 06520;*

*Clark University, Worcester, Massachusetts 01610;*

*and Institute of Atomic Physics, Bucharest-Magurele, Romania*

(Received 25 March 1998)

Octupole states have been studied systematically in the deformed actinide nuclei  $^{230}\text{Th}$ ,  $^{234,236,238}\text{U}$ ,  $^{240}\text{Pu}$ ,  $^{246}\text{Cm}$ , and  $^{250}\text{Cf}$  using the interacting boson approximation I. Parameters for the positive parity cores were set by reproducing data from the ground state and  $\gamma$ -vibration bands with the extended consistent- $Q$  formalism. A prescription for setting the parameter  $\epsilon_f$  systematically was adopted for the calculations of the octupole bands. The ordering of the  $K^\pi=0^-, 1^-,$  and  $2^-$  bands and the behavior of many  $E1$  and  $E3$  transitions are well reproduced with a narrow range of parameters, particularly when the existence of a  $N=164$  subshell gap is assumed. It is predicted that in  $^{246}\text{Cm}$  and  $^{250}\text{Cf}$  the  $K^\pi=3^-$  octupole states built on the ground state are located above 6 MeV and are strongly fragmented. [S0556-2813(98)02509-6]

PACS number(s): 21.60.Fw, 21.10.Re, 23.20.Lv, 27.90.+b

## I. INTRODUCTION

Low-lying collective negative parity states in even-even nuclei of the actinide region are generally interpreted either as octupole vibrational states or as rotational states of a statically octupole deformed nucleus. Despite considerable theoretical and experimental effort during the last fifteen years, there are still many open questions about octupole collectivity in this region. For example, in several Ra and Th isotopes which appear to be stably octupole deformed at high spins, the boundary between static and dynamic deformations is blurred at low spins where the experimental evidence suggests a softening of the octupole deformation. However, the negative parity bands of several  $A \geq 228$  nuclei were successfully explained using RPA calculations [1] as bands built on octupole vibrations. These bands are now considered to be some of the best examples of octupole vibrational behavior in quadrupole deformed nuclei.

Octupole vibrations can be described in the framework of the interacting boson approximation (IBA) [2] by introducing an  $f$  boson of angular momentum  $L^\pi=3^-$  in addition to the usual  $s$  ( $L^\pi=0^+$ ) and  $d$  ( $L^\pi=2^+$ ) bosons [3]. Barfield *et al.* [4] performed a systematic study of the  $sdf$  Hamiltonian and its parameters in the deformed rare-earth region. In Ref. [5], a new parameter constraint was placed on the  $sdf$  Hamiltonian by interpreting the energy of the  $f$  boson as the centroid of the low-lying octupole strength. Even with this constraint, a detailed description of octupole bands in the deformed rare-earth nuclei was achieved with smoothly varying parameters. Data on energies,  $E3$  strength distributions, and  $E1$  transition strengths for the  $K^\pi=0^-, 1^-,$  and  $2^-$  bands were reproduced satisfactorily. The calculations predict that in several of these nuclei the  $E3$  strength associated with the  $K=3$  octupole states is located at energies above 6 MeV, an energy range usually associated with the low-energy octupole resonance (LEOR) [6].

In the present article, we apply the same prescription used

in Ref. [5] to study the applicability of the IBA-1 with one  $f$  boson to octupole bands in the deformed actinide region. Since the existence of a spherical subshell closure at  $N=164$  has been proposed [7] (in addition to the major shell closure assumed to occur at  $N=184$ ), we also examine the role of the boson number on the selection of parameters.

## II. INTERACTING BOSON MODEL DESCRIPTION OF THE POSITIVE PARITY STATES

In order to describe the positive parity levels we use the IBA-1 in the extended consistent  $Q$  formalism (ECQF), in which the Hamiltonian takes the form [8]:

$$H_{sd} = \epsilon_d n_d + a_2 Q_d Q_d, \quad (1)$$

where

$$Q_d = (s^\dagger \tilde{d} + d^\dagger s) + \chi_2 (d^\dagger \tilde{d})^{(2)}, \quad (2)$$

and the electric quadrupole operator  $T(E2) = e_2 Q_d$ .

In typical deformed nuclei, one often uses the simpler consistent  $Q$  formalism (CQF) with  $\epsilon_d=0$ . However, it was recently shown [9] that finite  $\epsilon_d$  values improve fits even for well-deformed rare-earth nuclei. For the deformed actinide calculations described here, we adopted the same fitting method introduced in Ref. [8] and used in Ref. [9] for the rare-earth region.

Equations (1) and (2) involve three parameters  $\epsilon_d$ ,  $\chi_2$ , and  $a_2$ , plus the boson number  $N_B$ , defined as half the sum of the numbers of valence protons and neutrons relative to the nearest closed shell. For protons, we consider the usual closed shell at  $Z=82$  and for neutrons,  $N=126$  and  $N=184$ . Following the suggestion of Ref. [7], we also search for evidence of the proposed spherical subshell closure at  $N=164$  by examining the plausibility of the parameter sets necessary to fit the data with and without the effect of this closure on the boson number.

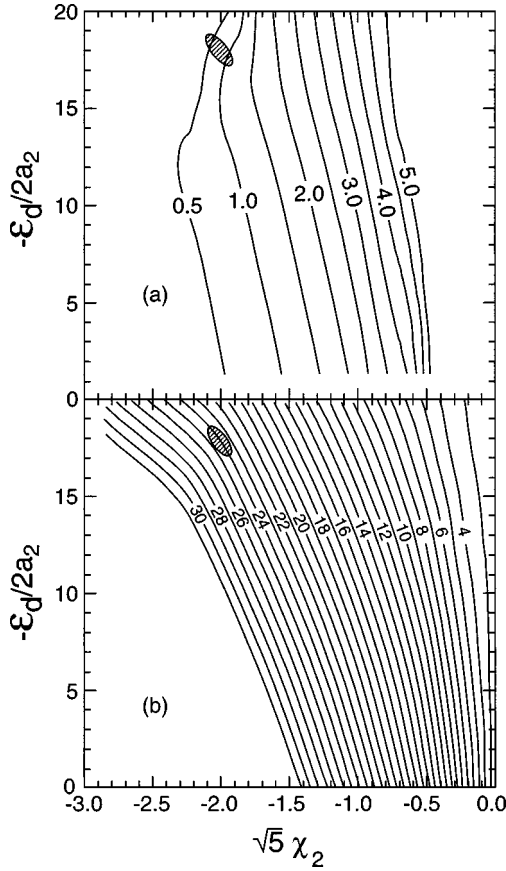


FIG. 1. Contour plots of (a)  $B(E2; 2_\gamma^+ \rightarrow 0_{g.s.}^+)/B(E2; 2_1^+ \rightarrow 0_{g.s.}^+) \times 10^3$  and (b)  $E(2_\gamma^+)/E(2_1^+)$  for boson number 21. The values of  $-\epsilon_d/2a_2$  and  $\chi_2 \times 5^{1/2}$  which are consistent with the experimental values of both quantities for  $^{250}\text{Cf}$  are indicated by the cross-hatched area.

The parameters were determined by fitting the energies of the states in the ground and  $\gamma$  bands—with a particular emphasis on the low spin states—and the ratio  $B(E2; 2_\gamma^+ \rightarrow 0_{g.s.}^+)/B(E2; 2_1^+ \rightarrow 0_{g.s.}^+)$ . The wave functions for a given boson number  $N_B$  depend only on two parameters  $\chi_2$  and  $\epsilon_d/a_2$ . Therefore, we can determine these two parameters by fitting energy ratios and  $B(E2)$  ratios. The absolute energy scale can then be set by adjusting  $\epsilon_d$  and  $a_2$  (keeping their ratio constant) and the absolute  $B(E2)$  values can be reproduced by adjusting the effective charge  $e_2$ .

This procedure can be performed using contour plots such as those for  $N_B=21$  shown in Fig. 1. This boson number corresponds to  $^{250}\text{Cf}$ , assuming the  $N=164$  subshell gap does not exist. The plots of  $B(E2; 2_\gamma^+ \rightarrow 0_{g.s.}^+)/B(E2; 2_1^+ \rightarrow 0_{g.s.}^+)$ , which is shown in Fig. 1(a), and  $E(2_\gamma^+)/E(2_1^+)$  [Fig. 1(b)] each include a cross-hatched area which shows the range of parameters which approximately reproduces the data on these two observables [0.00676(119) and 24.2, respectively]. It is clear that  $\epsilon_d/a_2$  must be nonzero to reproduce the data and  $\chi_2$  must fall near  $-2/5^{1/2}$ . Once these values are set,  $\epsilon_d$  and  $a_2$  are selected to reproduce  $E(2_1^+)$ .

Table I gives the values of the parameters for the positive parity states for the nuclei studied here. The effective charges  $e_2$  were selected to reproduce the experimental data for  $B(E2; 2_1^+ \rightarrow 0_{g.s.}^+)$ . A comparison of the calculated energies for ground and  $\gamma$  bands with the data are presented in the

TABLE I. IBA parameters for positive parity states.

Nucleus	$N_B$	$\epsilon_d$ (keV)	$a_2$ (keV)	$\chi_2$	$e_2$ ( $e$ b)
$^{230}\text{Th}$	11	180	-16.5	-0.84	0.20
$^{234}\text{U}$	13	80	-18.0	-0.77	0.19
$^{236}\text{U}$	14	80	-18.5	-0.69	0.18
$^{238}\text{U}$	14	50	-19.5	-0.77	0.18
	15	80	-18.0	-0.77	0.18
$^{240}\text{Pu}$	15	120	-17.0	-0.91	0.18
	16	120	-16.0	-0.91	0.17
$^{246}\text{Cm}$	14	80	-19.5	-0.77	0.21
	19	140	-16.0	-0.72	0.16
$^{250}\text{Cf}$	14	100	-16.5	-0.89	0.21
	21	350	-10.5	-0.94	0.15

upper panels of Figs. 2–8. The first excited  $K^\pi=0^+$  bands are not shown, and the calculated energies for these bands are 300–500 keV higher than the experimental values. This latter result is not unusual—it is a feature of many IBA calculations [8]. The experimental and calculated values of the ratio  $R=B(E2; 2_\gamma^+ \rightarrow 0_{g.s.}^+)/B(E2; 2_1^+ \rightarrow 0_{g.s.}^+)$  are also given in the upper panels of Figs. 2–8.

The IBA parameters fall into narrow ranges for almost all the nuclei studied here. The one exception is  $^{250}\text{Cf}$ , which for  $N_B=21$  (the boson number if the  $N=164$  subshell gap does not exist) yields  $\epsilon_d=350$  keV and  $a_2=-10.5$  keV. These values are far out of the ranges set by the other isotopes calculated here: 80 to 180 keV for  $\epsilon_d$  and  $-16.0$  to  $-21.5$  keV for  $a_2$ . If the  $N=164$  subshell gap does exist, as suggested in Ref. [7], then  $N_B=14$  for  $^{250}\text{Cf}$ . The contour plots for  $B(E2; 2_\gamma^+ \rightarrow 0_{g.s.}^+)/B(E2; 2_1^+ \rightarrow 0_{g.s.}^+)$  and  $E(2_\gamma^+)/E(2_1^+)$  with  $N_B=14$  which are given in Fig. 9 show that a much smaller  $\epsilon_d/2a_2$  ratio and, therefore, a smaller value of  $\epsilon_d$  are needed to reproduce the data. In fact, the values of  $\epsilon_d$  and  $a_2$  obtained for  $N_B=14$  ( $\epsilon_d=100$  keV,  $a_2=-16.5$  keV) fall within the ranges defined by the other nuclei in the present study. This result suggests that the  $N=164$  spherical subshell gap indeed exists, particularly since  $^{250}\text{Cf}$  would be the most sensitive to the presence of the gap among the nuclei studied here because its boson number is most strongly affected. In the case of  $^{246}\text{Cm}$ , the boson number changes by five (from 19 to 14) if the  $N=164$  gap exists, but the parameters obtained for these two boson numbers are quite similar. In  $^{238}\text{U}$  and  $^{240}\text{Pu}$ , the boson number changes by only one if the  $N=164$  gap exists, so almost no change in parameters occurs. The boson numbers are unaffected by the possible subshell closure in  $^{230}\text{Th}$ ,  $^{234}\text{U}$ , and  $^{236}\text{U}$ . The parameters for calculations which do and do not assume the subshell gap are given in Table I, and the results of both sets of calculations are given in Figs. 5–8.

The behavior of the  $e_2$  values suggests that an effective number of bosons intermediate between those given by the assumptions of the  $N=164$  and  $184$  shell closures would be most appropriate. When the existence of the  $N=164$  subshell closure is assumed, the effective charges necessary to reproduce the data in  $^{246}\text{Cm}$  and  $^{250}\text{Cf}$  (0.21  $e$  b) are higher than those in  $^{230}\text{Th}$  and  $^{234,236,238}\text{U}$  (0.18–0.20  $e$  b). If no subshell closure is assumed, effective charges of 0.16 and 0.15  $e$  b—lower than in Th and U—are obtained for  $^{246}\text{Cm}$

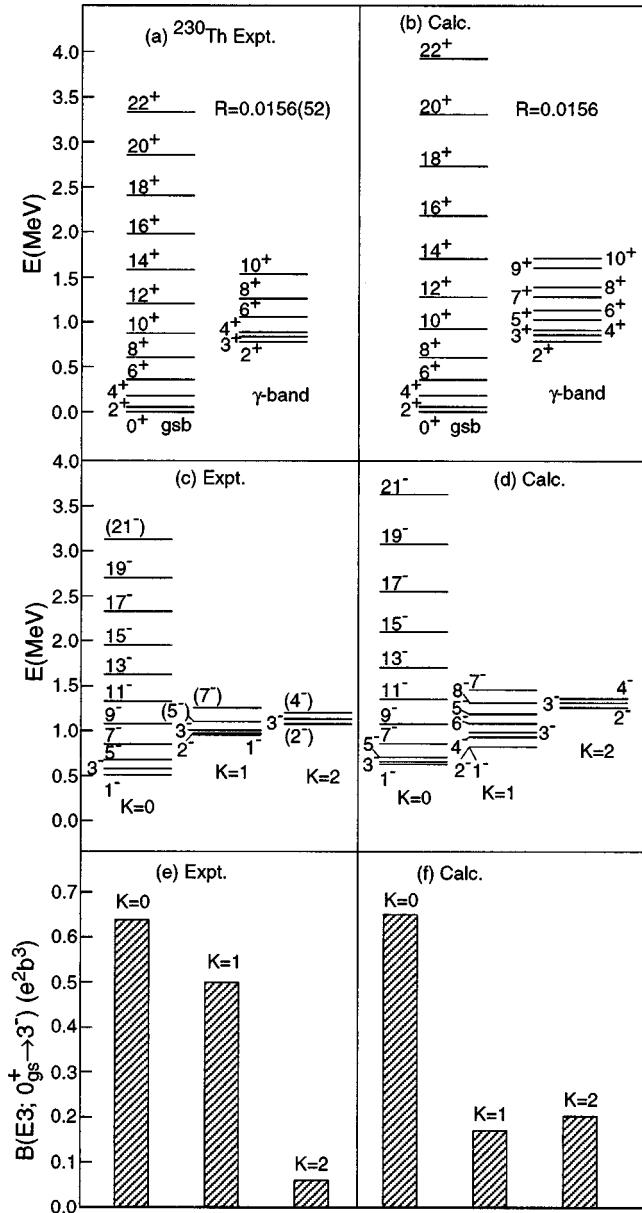


FIG. 2. (a) Experimentally observed values of the energies for ground state and  $\gamma$ -vibration bands and the ratio  $R=B(E2;2_1^+ \rightarrow 0_{g.s.}^+)/B(E2;2_1^+ \rightarrow 0_{g.s.}^+)$  in  $^{230}\text{Th}$ ; (b) calculated values of the energies for ground state and  $\gamma$ -vibration bands and the ratio  $R$ ; (c) experimentally observed energies for  $K^\pi=0^-, 1^-,$  and  $2^-$  octupole bands; (d) calculated energies for  $K^\pi=0^-, 1^-,$  and  $2^-$  octupole bands; (e) experimentally observed  $B(E3;0_{g.s.}^+ \rightarrow 3^-)$  values for the  $J^\pi=3^-$  members of the  $K^\pi=0^-, 1^-,$  and  $2^-$  octupole bands; (f) calculated  $B(E3;0_{g.s.}^+ \rightarrow 3^-)$  values for the  $J^\pi=3^-$  members of the  $K^\pi=0^-, 1^-,$  and  $2^-$  octupole bands. Data are taken from Refs. [10–12].

and  $^{250}\text{Cf}$ , respectively. An intermediate effective boson counting scheme would yield a constant  $e_2$  value across the region. This effective boson number would be similar to that deduced by Scholten [24] to take into account the subshell closure at  $Z=64$  in the rare-earth region. However, in the present work we will not consider effective boson numbers as in Ref. [25] and we will limit ourselves to the assumptions of  $N=164$  and  $184$  shell closures.

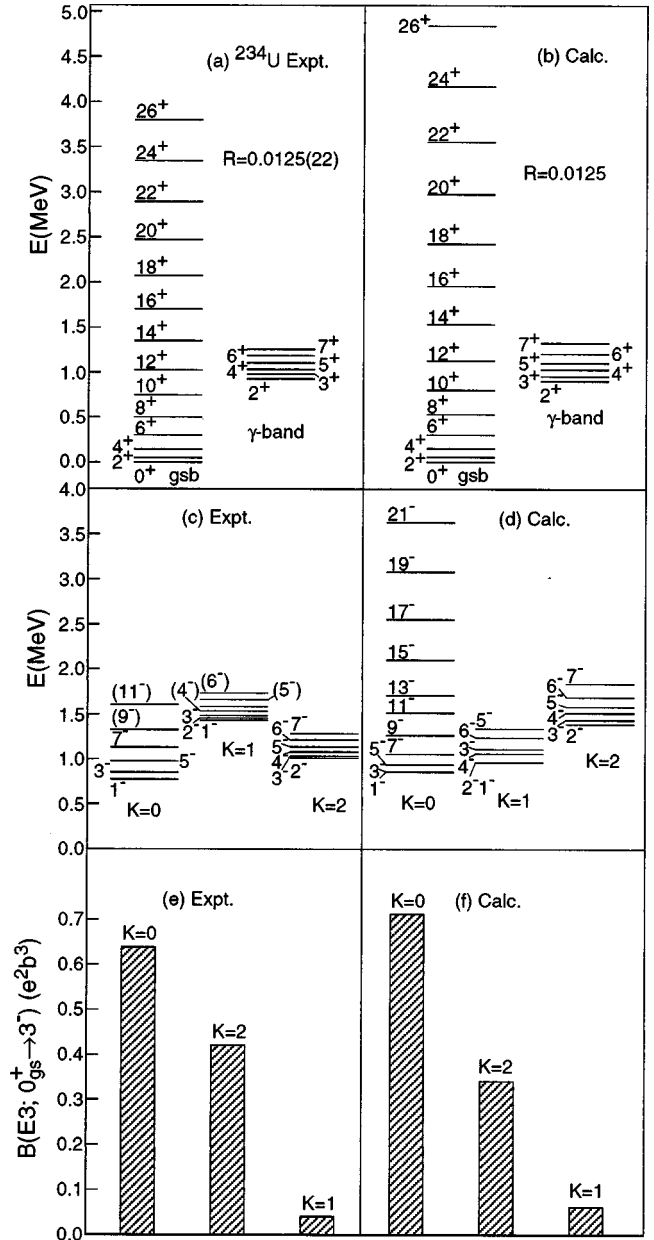


FIG. 3. Similar to Fig. 2 for  $^{234}\text{U}$ . Data are taken from Refs. [13, 14].

### III. OCTUPOLE STATES IN THE IBA-1 $sdf$ MODEL

Octupole states are described in the IBA-1 by adding a single  $f$  boson with  $L=3$  to the usual  $s$ - $d$  boson model space [3,4]. The total number of  $s$ ,  $d$ , and  $f$  bosons is conserved, and the number of  $f$  bosons  $n_f$  can be zero or one, for positive and negative parity states, respectively. The Hamiltonian is

$$H = H_{sd} + H_f + V_{sdf}, \quad (3)$$

where  $H_{sd}$  describes the positive parity core,  $H_f$  is the  $f$ -boson Hamiltonian, and  $V_{sdf}$  describes the  $f$ - $sd$  interaction. The  $f$ -boson Hamiltonian  $H_f$  is given by

$$H_f = \epsilon_f n_f, \quad (4)$$

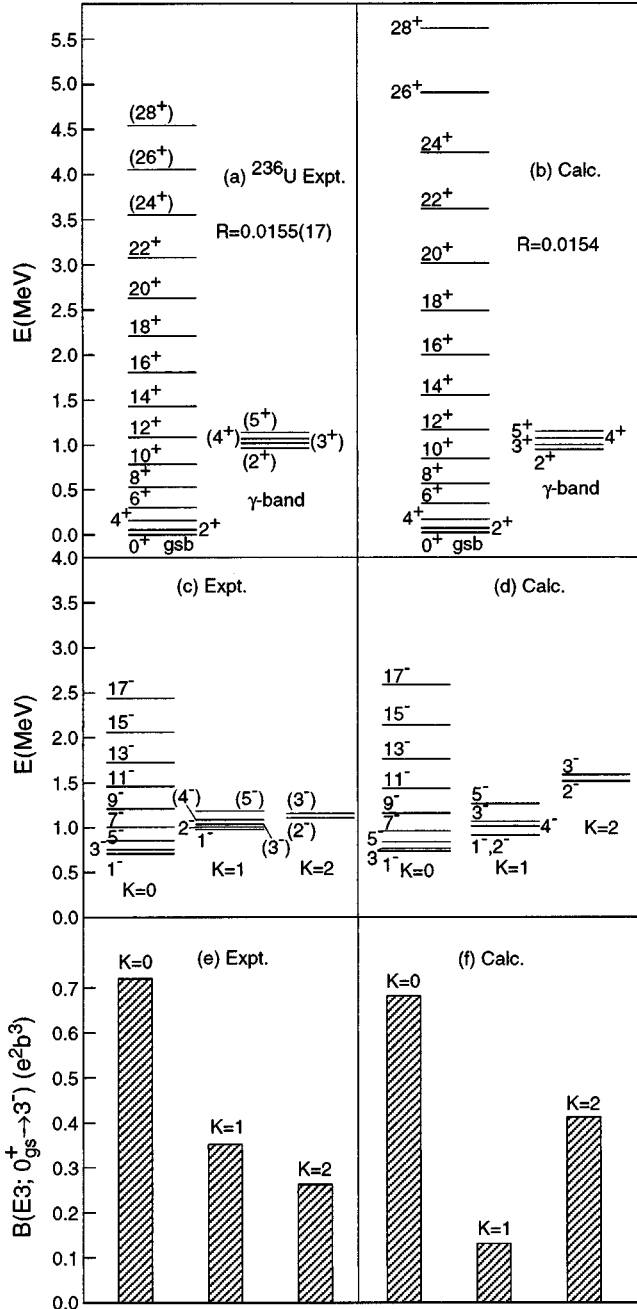


FIG. 4. Similar to Fig. 2 for  $^{236}\text{U}$ . Data are taken from Refs. [13, 15].

where  $\epsilon_f$  is the  $f$ -boson energy. The interaction term  $V_{sdf}$  used here is identical to that used in Refs. [4, 5]:

$$V_{sdf} = A_1 L_d L_f + A_2 Q_d Q_f + A_3 :E_{df}^+ E_{df}:, \quad (5)$$

where

$$L_f = 2\sqrt{7}(f^\dagger \tilde{f})^{(1)}, \quad (6)$$

$$Q_f = -2\sqrt{7}(f^\dagger \tilde{f})^{(2)}, \quad (7)$$

and the normal-ordered exchange term

$$:E_{df}^+ E_{df}: = 5:(d^\dagger \tilde{f})^{(3)}(f^\dagger \tilde{d})^{(3)}:. \quad (8)$$

Here, as in Ref. [5], we interpret  $\epsilon_f$  as the energy of the low-energy octupole state (LEOS). Since the LEOS is fragmented in deformed nuclei, the energy of the LEOS (and therefore  $\epsilon_f$ ) in a deformed nucleus was taken to be the centroid of the observed octupole strength, which is given by [26]

$$C = \frac{\sum_i E_i B(E3; 0_{g.s.}^+ \rightarrow 3_i^-)}{\sum_i B(E3; 0_{g.s.}^+ \rightarrow 3_i^-)}, \quad (9)$$

where  $E_i$  is the energy of the  $i$ th  $J^\pi = 3^-$  state. To set  $\epsilon_f$  in each nucleus we used the systematic behavior of the observed energy centroids, so that inaccuracies introduced by the poor quality of data in individual nuclei are minimized.

The systematic behavior of the octupole centroids for the deformed actinide region ( $N > 140$ ) as a function of neutron number is shown in Fig. 10. This information comes from inelastic scattering and Coulomb excitation measurements performed with protons, deuterons, and  $\alpha$  particles. Experimental studies in which more than one  $3^-$  state was measured were included. There are experimental errors inherent in the measurements of the  $B(E3; 0_{g.s.}^+ \rightarrow 3^-)$  values, and these translate into errors in the centroid energies. However, these errors are always less than 50 keV, so we have not included them in the figures. We include all  $3^-$  states, even if they are not assigned to octupole bands by the experimenters. There is some variation in the quality of the data; however, the compilation is sufficient for the purposes of the present work.

Throughout the deformed actinide region, the energy of the octupole centroid appears to increase as a function of neutron number. This behavior can be explained in terms of a schematic description of octupole states [29–31]. In spherical nuclei, octupole states consist primarily of two quasiparticle excitations involving the unique parity orbit and the normal parity orbit with three fewer units of both total and orbital angular momentum than the unique parity orbit. For the  $N > 126$  major shell, the relevant neutron orbits are  $j_{15/2}$  and  $g_{9/2}$ . Near  $N = 126$ , the  $g_{9/2}$  orbit is actually the lowest in the major shell. As neutrons are added at the beginning of the shell, the  $g_{9/2}$  orbit fills and the energy of the octupole state falls. By  $N = 140$ , the  $g_{9/2}$  orbit is full and the  $j_{15/2}$  orbit is beginning to fill, causing the energy of the octupole state (or centroid of octupole states) to increase. The onset of quadrupole deformation at  $N = 134$  results in the breaking of the degeneracies of the magnetic substates of the single particle orbits; however, the centroids of the orbits remain roughly the same, and this general description of the behavior of the octupole centroid remains valid, even in deformed nuclei.

We use the relationship between the octupole centroid energy and the neutron number to set  $\epsilon_f$ . The dashed line drawn in Fig. 10 from  $N = 140$  to  $N = 152$  provides a prescription for  $\epsilon_f$  (with  $\epsilon_f = E_{\text{LEOS}}$ ) and is given by the equation

$$E_{\text{LEOS}} = [(34.37) \times N - 4043] \text{ keV}. \quad (10)$$

This equation gives a reasonable description of the systematic behavior of octupole centroids above  $N = 138$ . The slope of this line, 34.37 keV, is similar to the 40 keV slope

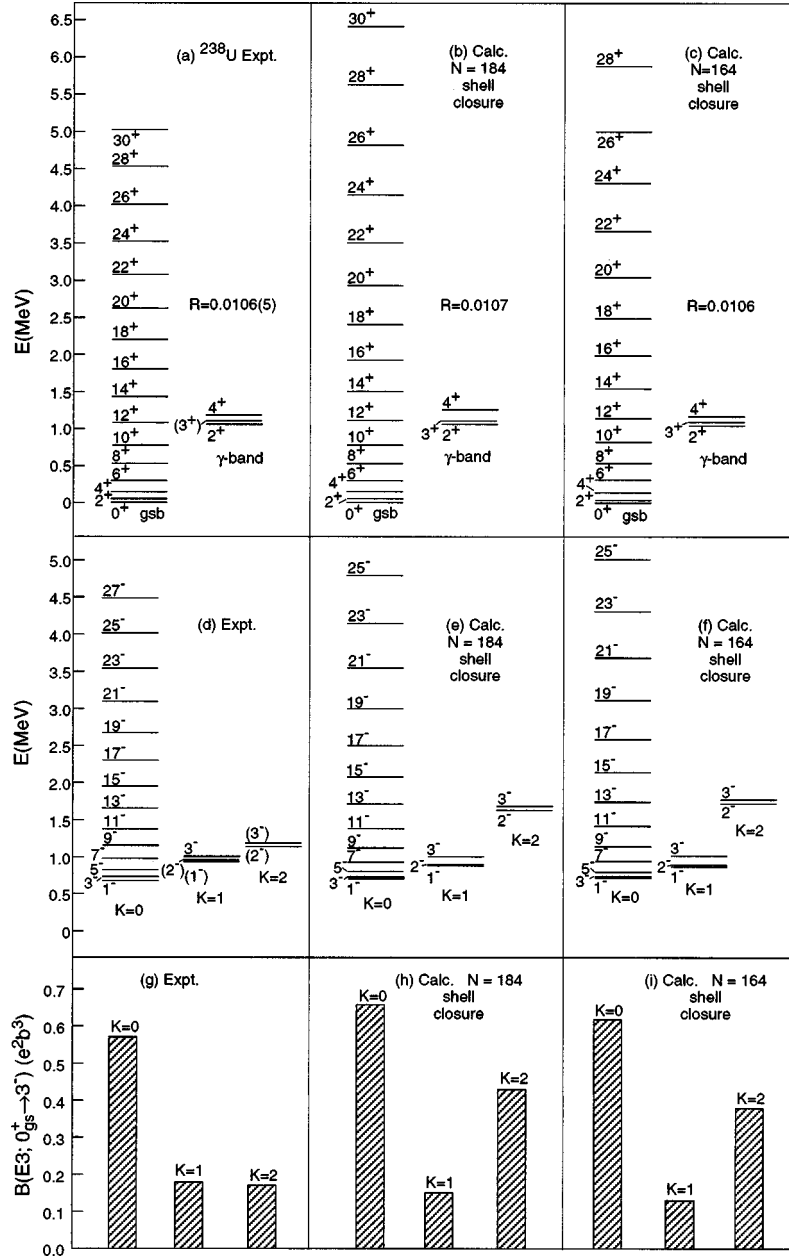


FIG. 5. (a) Experimentally observed values of the energies for ground state and  $\gamma$ -vibration bands and the ratio  $R=B(E2;2_1^+ \rightarrow 0_{g.s.}^+)/B(E2;2_2^+ \rightarrow 0_{g.s.}^+)$  in  $^{238}\text{U}$ ; (b) calculated values of the energies for ground state and  $\gamma$ -vibration bands and the ratio  $R$  assuming the  $N=184$  shell closure; (c) similar to (b) but assuming the  $N=164$  subshell closure; (d) experimentally observed energies for  $K^\pi=0^-, 1^-,$  and  $2^-$  octupole bands; (e) calculated energies for  $K^\pi=0^-, 1^-,$  and  $2^-$  octupole bands assuming the  $N=184$  shell closure; (f) similar to (e) but assuming the  $N=164$  subshell closure; (g) experimentally observed  $B(E3;0_{g.s.}^+ \rightarrow 3^-)$  values for the  $J^\pi=3^-$  members of the  $K^\pi=0^-, 1^-,$  and  $2^-$  octupole bands; (h) calculated  $B(E3;0_{g.s.}^+ \rightarrow 3^-)$  values for the  $J^\pi=3^-$  members of the  $K^\pi=0^-, 1^-,$  and  $2^-$  octupole bands assuming the  $N=184$  shell closure; (i) similar to (h) but assuming the  $N=164$  subshell closure. Data are taken from Refs. [16–18].

found in the rare-earth region [5]. This is not surprising since the structures of the valence neutron shells in the two regions are quite similar.

The  $E3$  transition rates are calculated with the operator [4]

$$T(E3) = e_3 [s^\dagger \tilde{f} + \chi_3 (d^\dagger \tilde{f})^{(3)} + \text{H.c.}] \quad (11)$$

where  $e_3$  is the boson octupole effective charge. The computer codes used for these calculations were PHINT and FBEM [32].

#### IV. CALCULATIONS OF ENERGIES AND $B(E3)$ VALUES FOR $K^\pi=0^-, 1^-, 2^-$ BANDS

In deformed nuclei, we expect four octupole vibrational bands to occur with  $K^\pi=0^-, 1^-, 2^-$ , and  $3^-$ . There is a considerable amount of data available for  $K^\pi=0^-, 1^-$ , and  $2^-$  octupole bands, but little or none on  $K^\pi=3^-$  octupole bands. In this section, we focus on  $K^\pi=0^-, 1^-$ , and  $2^-$  bands.  $K^\pi=3^-$  bands are discussed in Sec. VI.

Calculations using the IBA-1 with an  $f$  boson were performed for the  $K^\pi=0^-, 1^-, 2^-$  bands of seven nuclei  $^{230}\text{Th}$ ,  $^{234,236,238}\text{U}$ ,  $^{240}\text{Pu}$ ,  $^{246}\text{Cm}$ , and  $^{250}\text{Cf}$ . These nuclei were se-

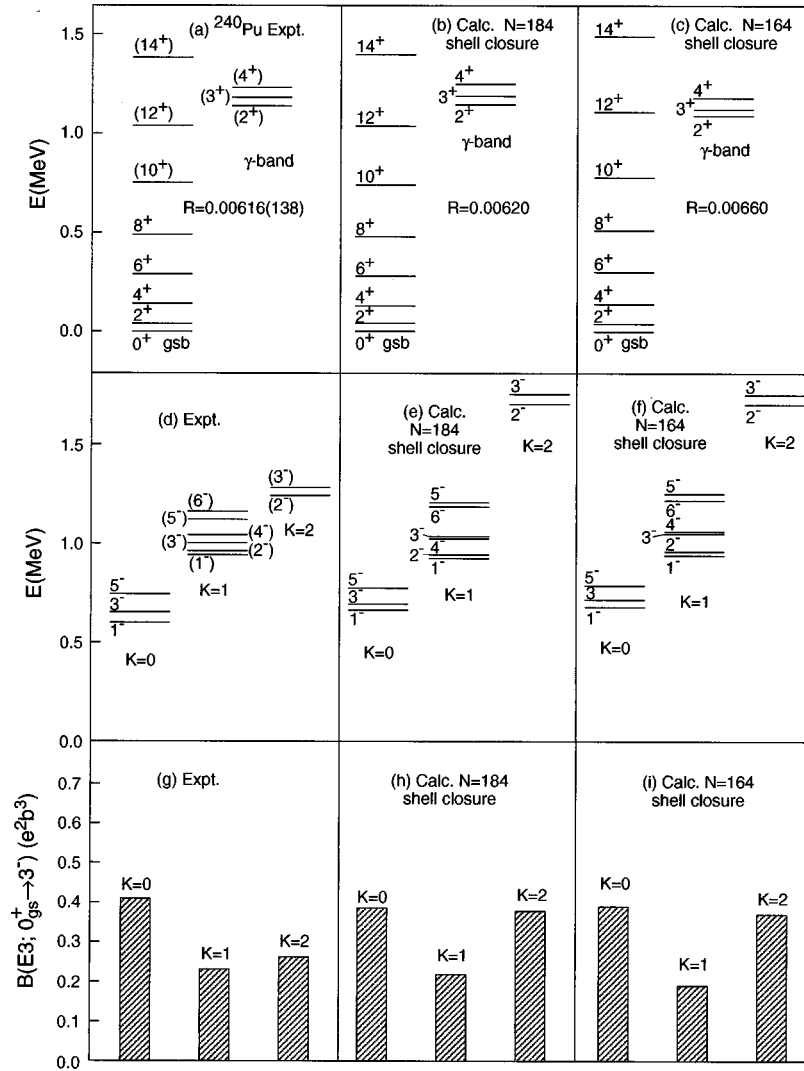


FIG. 6. Similar to Fig. 5 for  $^{240}\text{Pu}$ . Data are taken from Refs. [10, 19].

lected because energy and  $B(E3)$  information was available for at least two of the these bands in each nucleus.

The ordering of the octupole bands depends strongly on shell structure. In the beginning of the deformed region, the band sequence is  $K^\pi=0^-, 1^-, 2^-$ . As the Fermi level increases, the sequence changes to  $1^-, 0^-, 2^-$  and then to  $2^-, 1^-, 0^-$  [1]. Of the seven nuclei examined here, the  $K^\pi=0^-$  band is lowest in five. In the other two,  $^{246}\text{Cm}$  and  $^{250}\text{Cf}$ , the  $K^\pi=2^-$  band is lowest.

There are four parameters which affect the calculations of the energies of the negative parity states (after the positive parity states have been set)  $\epsilon_f$  [Eq. (4)] and  $A_1, A_2,$  and  $A_3$  [Eq. (5)]. The parameter  $\epsilon_f$  is set with the prescription described in Sec. III. Once this is set, the structure is primarily given by the parameters  $A_2$  and  $A_3$ . The ratio  $A_2/A_3$  determines the ordering of the octupole bands of different  $K$  values: when this ratio is small, the order is  $K^\pi=0^-, 1^-, 2^-$ ; for large  $A_2/A_3$ , the order is  $K^\pi=2^-, 1^-, 0^-$ . Values for these parameters are listed in Table II. The ordering of the bands of different  $K^\pi$  is practically independent of the  $A_1L_dL_f$  term. This ‘‘Coriolis-like’’ term does affect the order of levels within the bands and it is useful for fine-tuning in some cases [4]; nevertheless, it has little influence on wave func-

tions and consequently does not significantly affect the transition probabilities. Given these facts, we have left  $A_1=0$  for the calculations here.

Calculations of the  $B(E3; 0_{g.s.}^+ \rightarrow 3^-)$  transition probabilities depend on two additional parameters  $e_3$  (the octupole effective charge) and  $\chi_3$ . We find that a single value of  $e_3$  ( $0.19 e b^{3/2}$ ) was sufficient to describe almost all of the  $E3$  transitions examined here, and we note that a single effective charge ( $e_3=0.076 e b^{3/2}$ ) also fits the data for deformed rare-earth nuclei [5] (the effective charge of  $0.20 e b^{3/2}$  listed in Ref. [5] was in error by a factor of  $\sqrt{7}$ ). There is some variation in  $\chi_3$ , however, it is similar to that determined for the deformed rare-earth nuclei in Ref. [5]. The values of  $\chi_3$  are listed in Table II.

The method used here for setting  $\epsilon_f$  as equal to the octupole centroid energy (as described in the previous section) is one way of introducing microscopic information into the IBA, which does not intrinsically include details of single particle configurations. From the behavior of the other parameters, it is clear that the importance of shell effects goes beyond the behavior of the octupole centroids. However, the present prescription for setting  $\epsilon_f$  significantly constrains the model, and in fact determines a *unique* parameter set ( $A_2$  and

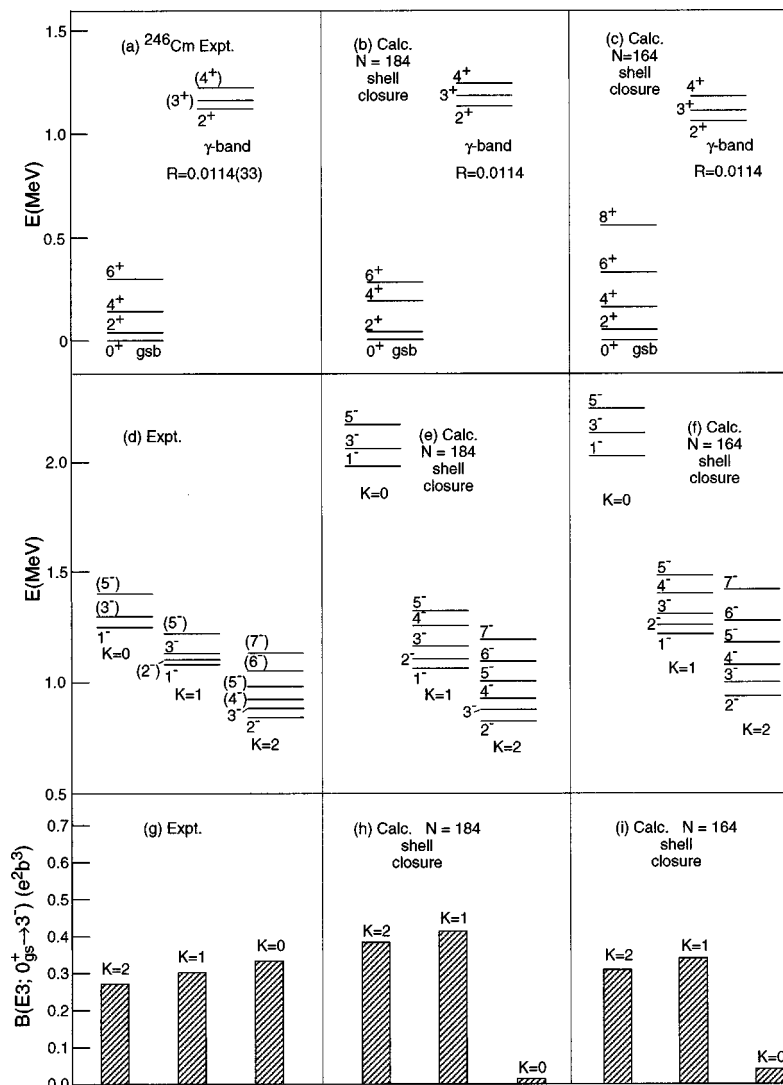


FIG. 7. Similar to Fig. 5 for  $^{246}\text{Cm}$ . Data are taken from Refs. [12, 20, 21].

$A_3$ ) for fitting the energies of octupole band states.

The results for the energies of states in the ground state,  $\gamma$  vibration, and octupole bands and the distribution of  $E3$  strength among the octupole bands are given in Figs. 2–8. For most of the nuclei shown here the calculations reproduce the data well. The calculated energy of the  $K^\pi=2^-$  band in  $^{236}\text{U}$ ,  $^{238}\text{U}$ , and  $^{240}\text{Pu}$  is 400–500 keV higher than the data, although the calculated band ordering reproduces the experimental ordering correctly.

In  $^{234}\text{U}$ , the experimental band order—with the  $K^\pi=0^-$  band lowest, the  $K^\pi=2^-$  band next lowest, and the  $K^\pi=1^-$  band third lowest—cannot be reproduced with the present model [4]. The calculated spectrum has the band ordering  $0^-, 1^-, 2^-$ , although none of the calculated bandhead energies differ by more than 500 keV from the experimental results. The observed band ordering in  $^{234}\text{U}$  may be caused in part by large admixtures of two quasiparticle configurations in the octupole states. Bjornholm *et al.* [33] performed a study of two quasineutron states in  $^{234}\text{U}$  using the  $^{233}\text{U}(d,p)$  reaction and measured large spectroscopic factors for the bandheads of the  $K^\pi=1^-$  and  $2^-$  octupole bands. A spectroscopic factor of 0.53 was measured for the  $\nu(7/2^-[743];5/2^+[633])$  configuration in the  $K^\pi=1^-$  band-

head, while a factor of 0.64 was measured for the  $\nu(7/2^-[743];3/2^+[631])$  configuration in the  $K^\pi=2^-$  bandhead. The large two quasiparticle components probably strongly influence the energies of  $K^\pi=1^-$  and  $2^-$  bands. These microscopic effects cannot be accommodated in the IBA-1, which accounts only for collective excitations. Similar two quasiparticle admixtures are likely to be responsible for some of the other shortcomings of the present calculations.

In  $^{246}\text{Cm}$ , the band ordering is correctly reproduced, although the calculated energy of the  $K^\pi=0^-$  bandhead is 700 keV higher than the observed energy for both sets of calculations. The  $K^\pi=0^-$  band has not been observed in  $^{250}\text{Cf}$ , but the calculated energies of the  $K^\pi=1^-$  and  $2^-$  bands are well reproduced by the calculations.

The fits to high spin states in the  $K^\pi=0^-$  bands of  $^{230}\text{Th}$  and  $^{238}\text{U}$  are not as good as at lower spins. The difficulty in fitting higher spin states might be attributable to the alignment of the octupole phonons, as discussed by Vogel [34]. As in the case of two quasiparticle admixtures in the bandheads discussed above, the IBA-1 cannot account for the microscopic alignment effect described by Vogel.

Even with the use of a single effective charge  $e_3$  for all

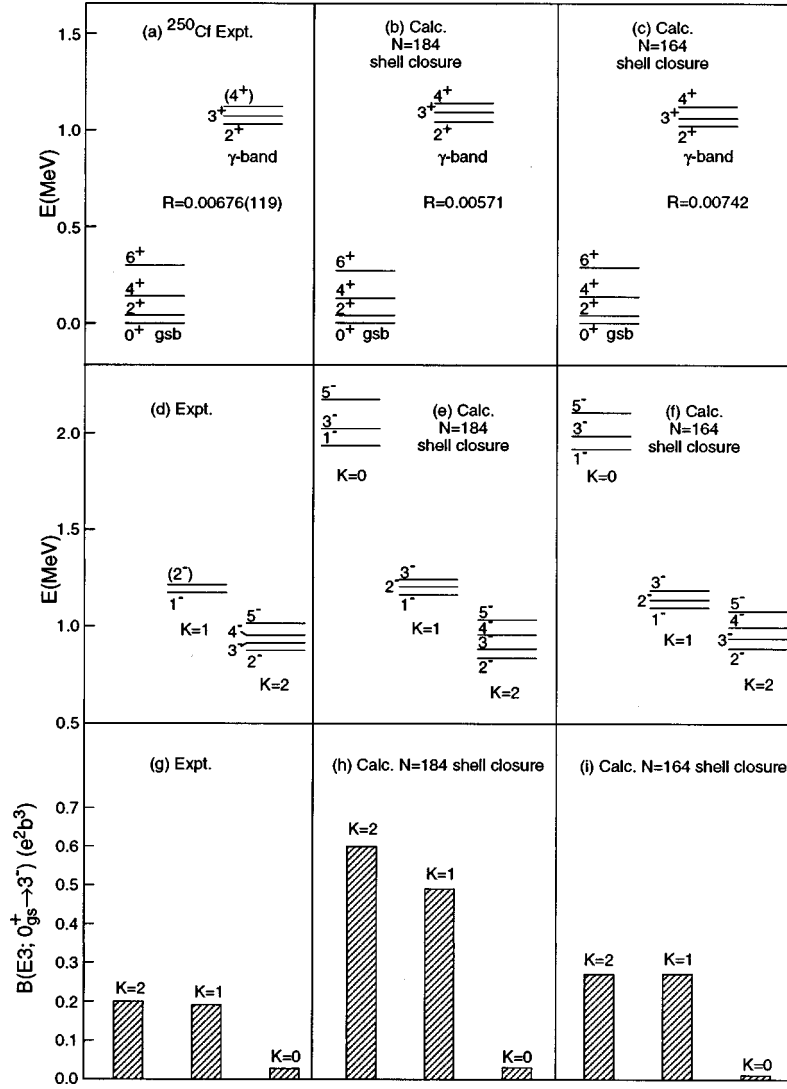


FIG. 8. Similar to Fig. 3 for  $^{250}\text{Cf}$ . Data are taken from Refs. [22, 23].

the nuclei studied here, the  $B(E3)$  relative and absolute strengths for the  $J^\pi = 3^-$  members of the  $K^\pi = 0^-, 1^-,$  and  $2^-$  bands are generally well reproduced in  $^{230}\text{Th}$ ,  $^{234,236,238}\text{U}$ , and  $^{240}\text{Pu}$ . In  $^{238}\text{U}$ , and  $^{240}\text{Pu}$ , the choice of  $N = 164$  or  $N = 184$  for the shell closure has little effect on the results of the calculations of the negative parity states, as is the case for positive parity states.

In  $^{246}\text{Cm}$ , the calculations give almost no  $E3$  strength in the  $K^\pi = 0^- J^\pi = 3^-$  state, while the data indicate that this state is the strongest among the  $K^\pi = 0^-, 1^-,$  and  $2^-$  octupole states. It is worth noting again that the calculated  $K^\pi = 0^-$  energies are also much higher than the observed energies, and it is quite possible that these two deviations are related. Choosing a boson number assuming an  $N = 164$  subshell closure (instead of simply assuming the  $N = 184$  major shell closure) does not improve the agreement.

In  $^{250}\text{Cf}$ , the only effect of calculating the boson number assuming the existence of the  $N = 164$  subshell closure is to change the  $E3$  effective charge required to reproduce the experimental octupole strength distribution. If the  $N = 164$  closure is considered (giving  $N_B = 14$ ), the effective charge which reproduces  $E3$  strengths in the other six nuclei considered here,  $e_3 = 0.19e b^{3/2}$ , can also reproduce the ob-

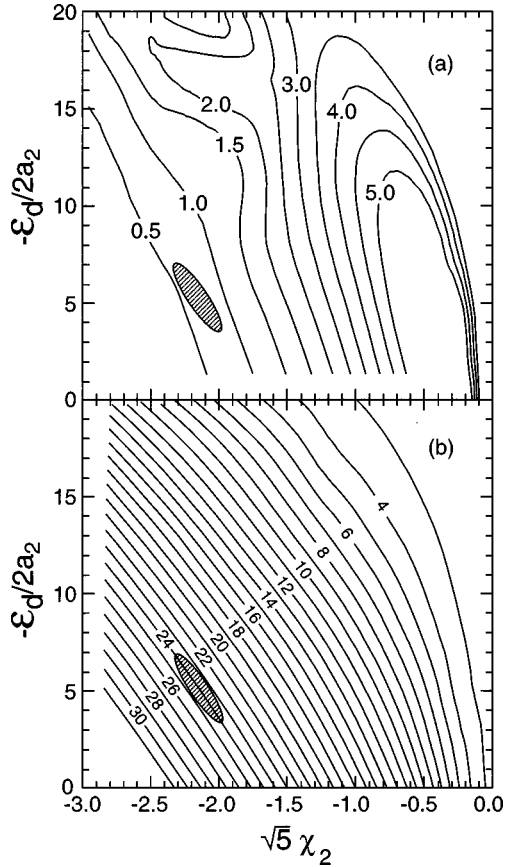
served strength distribution in  $^{250}\text{Cf}$ . Without the  $N = 164$  closure (so that  $N_B = 21$ ), a significantly smaller effective charge is required.

The present results for the IBA parameters necessary to reproduce the data are suggestive of the existence of a  $N = 164$  subshell closure, but this evidence is certainly not definitive. This issue will not be finally settled until measurements of  $E(2_1^+)$  and  $B(E2; 2_1^+ \rightarrow 0_{g.s.}^+)$  are performed for  $N \approx 164$  nuclei, as suggested in Ref. [7].

### V. E1 TRANSITIONS

The strengths of electric dipole transitions from octupole vibration states depend not only on the structure of the octupole states but also on small admixtures of the giant dipole resonance in the octupole states [35]. In the present work, as in the calculations of octupole states in the deformed rare-earth region in Ref. [5], we calculate  $E1$  transitions using an operator which includes the effect of small giant dipole resonance admixtures [35]

$$T_{sdf}^{(E1)} = e_1 [(d^\dagger f + d f^\dagger)^{(1)} + \chi_1 O_1 + \chi'_1 O'_1], \quad (12)$$

FIG. 9. Similar to Fig. 1 but for  $N_B = 14$ .

where  $O_1$  and  $O'_1$  are two-body terms. It was found in Ref. [37] that in order to reproduce branching ratios given by the Alaga rules for pure states of good  $K$  quantum number, the parameters  $\chi_1$  and  $\chi'_1$  must approximately satisfy the relation  $\chi_1 = 2\chi'_1$ . The same parameters also reproduce the  $E1$  branching ratios in rare-earth nuclei, including those cases where there are significant deviations from the Alaga rule.

We first analyze branching ratios of  $E1$  transitions, for which the  $E1$  effective charge  $e_1$  cancels out, in order to focus on the parameters  $\chi_1$  and  $\chi'_1$ . To satisfy the Alaga rule

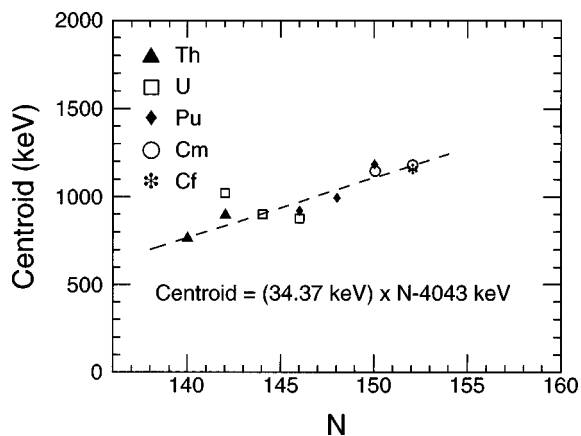


FIG. 10. Octupole centroids [as defined in Eq. (9)] graphed against the neutron number  $N$  for  $N = 140$ – $152$ . The data are from Refs. [10, 13, 16, 20, 22, 27, 28] and the dashed line is discussed in the text.

TABLE II. IBA parameters for negative parity states.

Nucleus	$\epsilon_f$ (keV)	$N_B$	$A_2$ (keV)	$A_3$ (keV)	$\chi_3$	$\chi_1 \times 10^2$	$\chi'_1 \times 10^2$
$^{230}\text{Th}$	0.77	11	-21	0	0.00	-3.00	-6.00
$^{234}\text{U}$	0.84	13	-27	-37	0.00	-2.60	-5.14
$^{236}\text{U}$	0.91	14	-31	-31	0.00	-2.54	-4.91
$^{238}\text{U}$	0.98	14	-37	-37	0.00	-2.54	-4.91
		15	-34	-34	0.00	-2.31	-4.68
$^{240}\text{Pu}$	0.98	15	-26	-5	+0.38	-2.42	-4.73
		16	-25	-5	+0.38	-2.42	-4.73
$^{246}\text{Cm}$	1.11	14	-40	-220	+0.38	-2.31	-4.68
		19	-45	-247	+0.76	-2.42	-4.73
$^{250}\text{Cf}$	1.18	14	-42	-222	+0.76	-2.31	-4.50
		21	-27	-200	+0.76	-2.42	-4.73

constraint, we make only small deviations from the ratio  $\chi_1/\chi'_1 = 2$  to fit the experimental  $E1$  ratios.

The parameters  $\chi_1$  and  $\chi'_1$  used for each nucleus are listed in Table II. The results of the calculations for  $E1$  transitions to the ground state bands are compared to the experimental data in Figs. 11–13. To simplify the reading of these figures, the results for  $^{230}\text{Th}$ ,  $^{234,238}\text{U}$ ,  $^{240}\text{Pu}$ , and  $^{246}\text{Cm}$  are located in the same panel location in each figure; the  $K^\pi = 0^-$  and  $1^-$  results for  $^{236}\text{U}$  and the  $K^\pi = 2^-$  results for  $^{250}\text{Cf}$  are shown in the lower right hand panels of the appropriate figures. The agreement between the calculated and experimental values shown in Figs. 11–13 is generally good. The branching ratios deviate—sometimes significantly—from the Alaga ratios due to mixing between octupole bands with different  $K$  values. The present calculations reproduce these deviations and the trend of the experimental values rather well. However, in some cases (e.g.,  $^{246}\text{Cm}$ ) the model does not reproduce the data very well. Even larger discrepancies occur for those branching ratios involving transitions to  $\gamma$ -vibrational bands (Table III). These discrepancies seem to be mainly due to the sensitivity of the calculated  $E1$  transition rates on different parameters in the operator. The two-body terms, which are large in absolute value, almost cancel each other to reproduce the small observed  $E1$  transition strengths. Another important contribution may come from single particle effects, which are discussed at the end of this section.

Data on absolute  $B(E1)$  values for some transitions in  $^{238}\text{U}$  are available [16] and are listed in Table IV. In particular,  $B(E1)$  has been measured for the decays of the  $J^\pi = 3^-$  states of the  $K^\pi = 0^-, 1^-, 2^-$  octupole bands to the  $2^+$  and  $4^+$  members of the ground state band. Table IV shows that the  $B(E1)$  values for these transitions in  $^{238}\text{U}$  can be well reproduced with a single effective charge for either shell closure assumption (0.026  $e$  fm for the assumption of a  $N = 164$  subshell closure, 0.025  $e$  fm without the subshell closure). The results with and without the subshell closure are quite similar, so only the results with the subshell closure are shown in Fig. 14. The  $^{238}\text{U}$  effective charge is determined by normalizing the calculated  $B(E1; 3^-_{K=0} \rightarrow 2^+_1)$  value to the data. The largest deviation of a calculated value from an experimental value occurs for the  $B(E1; 3^-_{K=2} \rightarrow 2^+_1)$  transition, where the calculation is nearly a factor of

TABLE III.  $B(E1; J_i^- \rightarrow J_{f1}^+)/B(E1; J_i^- \rightarrow J_{f2}^+)$  values for transitions to  $\gamma$  bands. Data are taken from Refs. [11, 14].

Nucleus	$K^\pi$	$J_i^\pi$	$J_{f1}^\pi$	$J_{f2}^\pi$	expt	calc
$^{230}\text{Th}$	$1^-$	$1^-$	$2_\gamma^+$	$2_1^+$	0.15(3)	2.70
	$2^-$	$2^-$	$3_\gamma^+$	$2_\gamma^+$	0.37(3)	0.42
		$2^-$	$2_\gamma^+$	$2_1^+$	2.56(19)	1.64
		$3^-$	$3_\gamma^+$	$2_\gamma^+$	1.37(17)	0
		$3^-$	$2_\gamma^+$	$2_1^+$	0.53(6)	0.045
$^{234}\text{U}$	$2^-$	$2^-$	$2_\gamma^+$	$2_1^+$	410(110)	29
	$4^-$	$3_\gamma^+$	$4_1^+$	55(40)	3.4	
		$3^-$	$2_\gamma^+$	$2_1^+$	40(14)	0

10 larger than the experimental value. The effective charge can also be used to predict  $B(E1; 1_{K=0}^- \rightarrow 0_{\text{g.s.}}^+)$  and  $B(E1; 1_{K=1}^- \rightarrow 0_{\text{g.s.}}^+)$ , which have not yet been reported (the report on a high resolution photon scattering experiment [38] did not give any results for states below 1782 keV). These predictions are also listed in Table IV.

A few absolute  $B(E1)$  values have also been measured in  $^{234,236}\text{U}$ . In  $^{234}\text{U}$ ,  $B(E1; 2_{K=2}^- \rightarrow 2_1^+)$  and  $B(E1; 2_{K=2}^- \rightarrow 2_\gamma^+)$  have been determined experimentally [14], allowing us to fix the effective charge for this nucleus by normalizing the calculated value of  $B(E1; 2_{K=2}^- \rightarrow 2_\gamma^+)$  to the experimental result and to predict  $B(E1; 1_{K=0}^- \rightarrow 0_{\text{g.s.}}^+)$  and  $B(E1; 1_{K=1}^- \rightarrow 0_{\text{g.s.}}^+)$ , as shown in Table IV. We have followed a similar procedure for  $^{236}\text{U}$ , where  $B(E1; 1_{K=0}^- \rightarrow 0_{\text{g.s.}}^+)$  and  $B(E1; 1_{K=0}^- \rightarrow 2_1^+)$  have been measured [15]. In this nucleus, the effective charge is fixed by normalizing the calculation for  $B(E1; 1_{K=0}^- \rightarrow 0_{\text{g.s.}}^+)$  to the experimental result, and a prediction for  $B(E1; 1_{K=1}^- \rightarrow 0_{\text{g.s.}}^+)$  is obtained (Table IV).

The  $E1$  transitions from the  $K^\pi = 0^-$   $J^\pi = 1^-$  state in  $^{236}\text{U}$  to members of the ground state band are three orders of magnitude weaker than the decays from the  $K^\pi = 0^-$   $J^\pi$

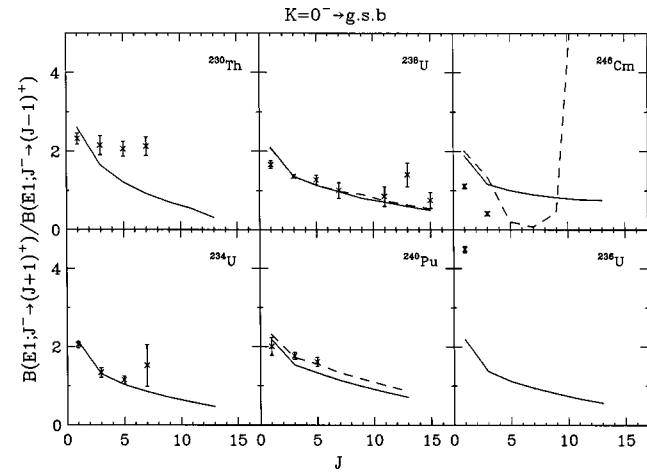


FIG. 11. Experimental and calculated  $E1$  branch ratios  $B(E1; J \rightarrow J+1)/B(E1; J \rightarrow J-1)$  for  $E1$  transitions from the  $K^\pi = 0^-$  band to the ground state band in  $^{230}\text{Th}$ ,  $^{234,236,238}\text{U}$ ,  $^{240}\text{Pu}$ , and  $^{246}\text{Cm}$ . Calculations assuming the existence of the  $N=164$  subshell gap are displayed as solid lines; calculations without this assumption are shown as dashed lines. Data are shown as crosses and are taken from Refs. [11, 14–19, 21, 36].

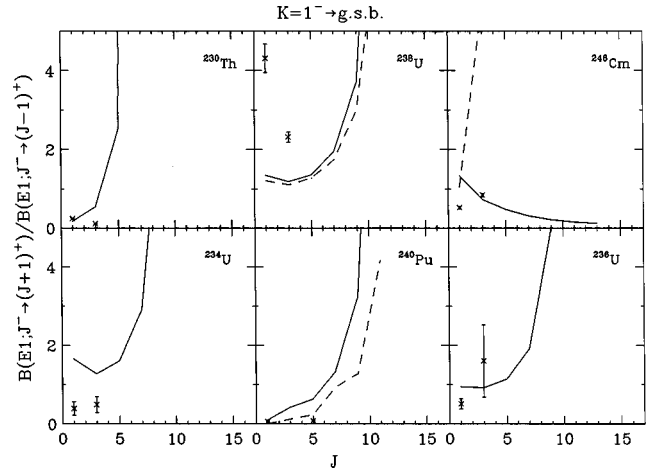


FIG. 12. Same as Fig. 11 for  $K^\pi = 1^-$  bands. Data are taken from Refs. [11, 14–19, 21, 36].

$= 3^-$  state to the ground state band members in  $^{238}\text{U}$ . This anomaly was noted earlier by Lederer [39]. However, the “collective”  $E1$  transitions induced by the dynamic dipole moment of the octupole-vibrating nucleus (a recent discussion of dipole moments in octupole-vibrating nuclei is given in Ref. [40]) are generally quite small compared to the Weisskopf unit (W.u.) (only  $10^{-4}$  W.u. in  $^{238}\text{U}$ ) and are therefore susceptible to interference, and cancellation, from single particle effects. Leander *et al.* [41] described this effect for the stably octupole deformed Ra and Th nuclei near  $A=222$  and for rare-earth nuclei in the vicinity of  $^{146}\text{Ba}$ .  $E1$  transitions are indeed much weaker in  $^{224}\text{Ra}$  and  $^{146}\text{Ba}$  than in their neighboring even-even isotopes [42,43], and the authors of Refs. [42, 43] attribute this to the shell effects described by Leander *et al.* We can speculate that in  $^{236}\text{U}$  we are observing a similar shell effect, but in a case of dynamic octupole deformation instead. A theoretical investigation of this possibility would be interesting.

The fact that sharply different values of the  $E1$  effective charge are required to reproduce absolute  $E1$  strengths in the

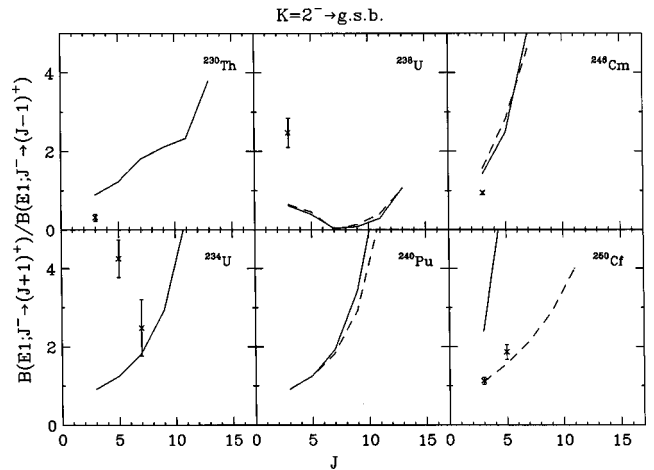


FIG. 13. Experimental and calculated  $E1$  branch ratios  $B(E1; J \rightarrow J+1)/B(E1; J \rightarrow J-1)$  for  $E1$  transitions from the  $K^\pi = 2^-$  band to the ground state band in  $^{230}\text{Th}$ ,  $^{234,238}\text{U}$ ,  $^{240}\text{Pu}$ ,  $^{246}\text{Cm}$ , and  $^{250}\text{Cf}$ . Calculations are displayed as in Figs. 11 and 12. Data are shown as crosses and are taken from Refs. [11, 14, 16, 17, 21, 23, 36].

TABLE IV.  $B(E1; J_i^- \rightarrow J_f^+)$  values. Data are taken from Refs. [14–16].

Nucleus	$e_1$ (e fm)	$e_1$ (e fm)	$K^\pi$	$J_i^\pi$	$J_f^\pi$	expt( $e^2 \text{fm}^2$ )	calc ( $e^2 \text{fm}^2$ )	calc ( $e^2 \text{fm}^2$ )
	$N=164$ shell	$N=184$ shell					$N=164$ shell	$N=184$ shell
$^{234}\text{U}$	0.057		$0^-$	$1^-$	$0_{\text{g.s.}}^+$		$2.6 \times 10^{-4}$	
			$1^-$	$1^-$	$0_{\text{g.s.}}^+$		$1.2 \times 10^{-4}$	
			$2^-$	$2^-$	$2_1^+$	$39(5) \times 10^{-7}$	$5.8 \times 10^{-6}$	
			$2^-$	$2^-$	$2_\gamma^+$	$1.7(5) \times 10^{-4}$	$1.7 \times 10^{-4}$	
$^{236}\text{U}$	0.00080		$0^-$	$1^-$	$0_{\text{g.s.}}^+$	$6.38(20) \times 10^{-8}$	$6.4 \times 10^{-8}$	
			$0^-$	$1^-$	$2_1^+$	$2.86(7) \times 10^{-7}$	$1.4 \times 10^{-7}$	
			$1^-$	$1^-$	$0_{\text{g.s.}}^+$		$1.1 \times 10^{-8}$	
$^{238}\text{U}$	0.026	0.025	$0^-$	$1^-$	$0_{\text{g.s.}}^+$		$8.3 \times 10^{-5}$	$8.6 \times 10^{-5}$
			$0^-$	$3^-$	$2_1^+$	$1.1(3) \times 10^{-4}$	$1.1 \times 10^{-4}$	$1.1 \times 10^{-4}$
			$0^-$	$3^-$	$4_1^+$	$1.4(4) \times 10^{-4}$	$1.5 \times 10^{-4}$	$1.5 \times 10^{-4}$
			$1^-$	$1^-$	$0_{\text{g.s.}}^+$		$8.9 \times 10^{-6}$	$7.9 \times 10^{-6}$
			$1^-$	$3^-$	$2_1^+$	$5.1(9) \times 10^{-6}$	$1.7 \times 10^{-5}$	$1.7 \times 10^{-5}$
			$1^-$	$3^-$	$4_1^+$	$1.3(2) \times 10^{-5}$	$1.8 \times 10^{-5}$	$1.9 \times 10^{-5}$
			$2^-$	$3^-$	$2_1^+$	$1.9(2) \times 10^{-7}$	$1.6 \times 10^{-6}$	$1.4 \times 10^{-6}$
			$2^-$	$3^-$	$4_1^+$	$4.7(6) \times 10^{-7}$	$9.5 \times 10^{-7}$	$8.7 \times 10^{-7}$

uranium isotopes illustrates an important point about the IBA. While the IBA can reproduce the relationships between the strengths of different  $E1$  transitions within a single nucleus, the single particle effects which play a large role in varying  $E1$  strengths from nucleus to nucleus are not included in the IBA. These effects must be included in an *ad hoc* way via the effective charge.

### VI. $K^\pi=3^-$ BANDS

While the data on energies and  $B(E3)$  values for  $K^\pi=0^-, 1^-, 2^-$  bands are nearly complete for the six nuclei discussed here, no collective  $K^\pi=3^-$  octupole bands have been firmly assigned in this mass region. Several  $K^\pi=3^-$  bands containing more than one state have been identified. Some appear to have noncollective two quasiparticle origin, and in other cases the band structure has not been unambiguously established. This situation is similar to that in the deformed rare-earth region, where the data on  $K^\pi=3^-$  octupole bands are limited and questionable [5].

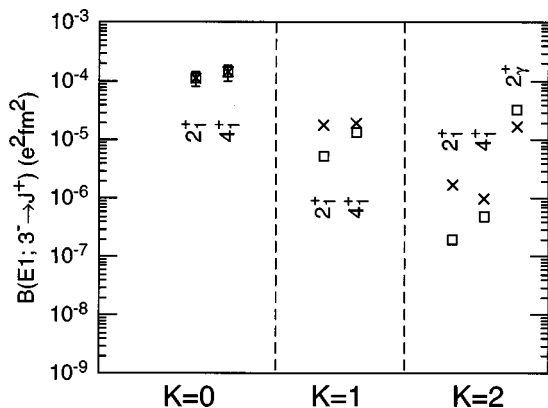


FIG. 14. A comparison of experimental (crosses) and calculated (squares)  $B(E1; 3^- \rightarrow J^+)$  values in  $^{238}\text{U}$ . The calculations were normalized so that  $B(E1; 3_{K=0}^- \rightarrow 2_1^+) = 1.1 \times 10^{-4} e^2 \text{fm}^2$ . The data are taken from Ref. [16].

Chan *et al.* [44] proposed that in  $^{232}\text{Th}$  the  $J^\pi=3^-, 4^-$ , and  $5^-$  states at 1182, 1218, and 1329 keV, respectively, are members of a  $K^\pi=3^-$  octupole band. The  $J^\pi=3^-$  member of the band was populated more weakly [ $B(E3; 0_{\text{g.s.}}^+ \rightarrow 3^-) = 0.039 e^2 \text{b}^3$ ] in the Coulomb excitation work of McGowan and Milner [28] than the  $K^\pi, J^\pi=0^-, 3^-$  state at 774 keV [ $B(E3; 0_{\text{g.s.}}^+ \rightarrow 3^-) = 0.54(5) e^2 \text{b}^3$ ]. However, Schmorak [15] notes that the only observed  $\gamma$  decay of the 1218 keV state is to the  $6_1^+$  state, so that the  $4^-$  assignment is likely to be incorrect. In addition, Schmorak offers no  $J^\pi$  assignment for the 1329 keV state. Hence, there is no band structure to support the  $K^\pi=3^-$  assignment for the 1182 keV state. In addition, Sood *et al.* [12] note that there is little support for several of the band assignments proposed by Chan *et al.*

In  $^{234}\text{U}$ , there is an apparent  $K^\pi=3^-$  band with  $J^\pi=3^-$  and  $4^-$  states at 1723 and 1762 keV, respectively, which has been observed via  $\beta$  decay [14,45]. The  $B(E3; 0_{\text{g.s.}}^+ \rightarrow 3^-)$  value for this band, as measured with the  $(d, d')$  reaction [13], is  $0.05(1) e^2 \text{b}^3$ , which can be compared to the values of  $0.64(4)$ ,  $0.42(4)$ , and  $0.04(1) e^2 \text{b}^3$  for the  $K^\pi=0^-, 2^-$ , and  $1^-$  octupole states at 849, 1024, and 1486 keV, respectively. Bjornholm *et al.* [45] assigned a  $5/2^+[642] - 1/2^- [530]$  two quasiproton configuration to this band, rather than a collective octupole interpretation, and the small value of  $B(E3; 0_{\text{g.s.}}^+ \rightarrow 3^-)$  for the  $J^\pi=3^-$  state is consistent with this assignment. Ardisson *et al.* [46] also identified a state at 1959 keV and assigned  $K^\pi, J^\pi=3^-, 3^-$  to this state on the basis of the strengths of the  $B(M1)$  transitions deexciting it. No associated band structure has yet been identified, so the  $K^\pi$  value cannot be confirmed. Ardisson *et al.* suggested a  $7/2^- [743] - 1/2^+ [631]$  two quasineutron configuration for this state on the basis of theoretical arguments.

An extended  $K^\pi=3^-$  band has been observed in  $^{236}\text{U}$  (states with  $J^\pi=3^-, 4^-, 5^-, 6^-$ , and  $7^-$  at energies of 1192, 1232, 1282, 1343, and 1413 keV, respectively) using the  $^{235}\text{U}(d, p)$  reaction by Katori *et al.* [47]. While this band is populated strongly in the  $(d, p)$  reaction, the  $J^\pi=3^-$  state was not observed at all in the  $^{236}\text{U}(d, d')$  study of Boyno

*et al.* [13]. Thus, Katori *et al.* argued that the band has a nearly pure  $7/2^- [743]-1/2^+ [631]$  two quasineutron configuration, and not a collective octupole structure.

In their  $\beta$  decay study of  $^{238}\text{Pu}$ , Winter *et al.* [48] proposed that a  $J^\pi=3^-$  state they observed at 1203 keV has  $K^\pi=3^-$  and a  $7/2^- [743]-1/2^+ [631]$  two quasineutron configuration instead of a collective octupole origin. No data on  $B(E3; 0_{\text{g.s.}}^+ \rightarrow 3^-)$  are available to test for collectivity.

Parekh *et al.* [49] proposed that a state observed in the  $^{240}\text{Pu}(d,d')$  reaction at 1675 keV [10] has  $J^\pi, K^\pi = 3^-, 3^-$ , even though no data on the angular distribution of the scattered deuterons is available. Therefore, this assignment is not adequately supported.

There is a much stronger candidate for a  $K^\pi=3^-$  octupole band in  $^{242}\text{Pu}$ , with  $J^\pi=3^-, 4^-,$  and  $5^-$  states located at 1019, 1064, and 1122 keV, respectively, and a large  $B(E3; 0_{\text{g.s.}}^+ \rightarrow 3^-)$  value. The  $J^\pi=3^-$  member of this sequence was measured in the Coulomb excitation study of McGowan *et al.* [50] to have  $B(E3; 0_{\text{g.s.}}^+ \rightarrow 3^-) = 0.45(7) e^2 b^3$  (compared to  $0.42(7) e^2 b^3$  for the  $J^\pi, K^\pi = 3^-, 0^-$  state) and in the  $(d,d')$  measurements of Elze *et al.* [27] to have  $B(E3; 0_{\text{g.s.}}^+ \rightarrow 3^-) = 0.74(11) e^2 b^3$  (compared to  $0.71(9) e^2 b^3$  for the  $J^\pi, K^\pi = 3^-, 0^-$  state). To firmly establish a  $K^\pi=3^-$  assignment, it would be necessary to eliminate the possibility that there is a lower spin member of this band by performing a complete spectroscopic study with a nonselective experimental probe such as  $(n,n'\gamma)$ .

Yates *et al.* [20] suggested that the  $J^\pi=3^-$  state at 1527 keV and the  $J^\pi=5^-$  state at 1652 keV in  $^{246}\text{Cm}$  are members of a  $K^\pi=3^-$  band. The  $J^\pi=3^-$  state was strongly populated in the  $(d,d')$  study of Yates *et al.* [ $B(E3; 0_{\text{g.s.}}^+ \rightarrow 3^-) = 0.18 e^2 b^3$ , compared to 0.33, 0.30, and  $0.27 e^2 b^3$  for the  $K^\pi=0^-, 1^-,$  and  $2^-$  octupole states, respectively]. However, Yates *et al.* also raised the possibility that the 1527 keV state might be a member of a  $K^\pi=0^-$  or  $1^-$  band in which the 1427 keV state would be the  $J^\pi=1^-$  member. Once again, further experimental work could clarify this situation.

A similar situation exists in  $^{250}\text{Cf}$ , where Ahmad *et al.* [22] suggested a  $K^\pi=3^-$  band assignment for the  $J^\pi=3^-$  state at 1427 keV and the  $J^\pi=5^-$  state at 1541 keV. The  $J^\pi=3^-$  state in this sequence is populated strongly in the  $(d,d')$  experiment of Ahmad *et al.* [ $B(E3; 0_{\text{g.s.}}^+ \rightarrow 3^-) = 0.13 e^2 b^3$ , compared to  $0.046(5), 0.19(2),$  and  $0.20(2) e^2 b^3$  for the  $K^\pi=0^-, 1^-,$  and  $2^-$  octupole states, respectively]. However, a detailed measurement of band structure in this nucleus would be necessary for this assignment to be convincing.

While any of the  $K^\pi=0^-, 1^-,$  or  $2^-$  octupole vibrational bands can be the lowest in the IBA-1, the  $K^\pi=3^-$  vibrational band is *always highest* in energy given realistic parameters. In the SU(3) limit of the  $sd$  Hamiltonian, the  $sd$ - $f$  quadrupole-quadrupole interaction breaks the degeneracy of the negative parity states and develops different bands characterized by the quantum number  $K$  [51]. The splitting of the different bands is proportional to  $K^2$  and to the strength of the  $sd$ - $f$  quadrupole-quadrupole interaction  $A_2$ . In particular, for large negative values of  $A_2$ , the energy of the  $J^\pi=3^-, K^\pi=3^-$  state based on the lowest SU(3) irreducible representation of the positive parity core is pushed up in

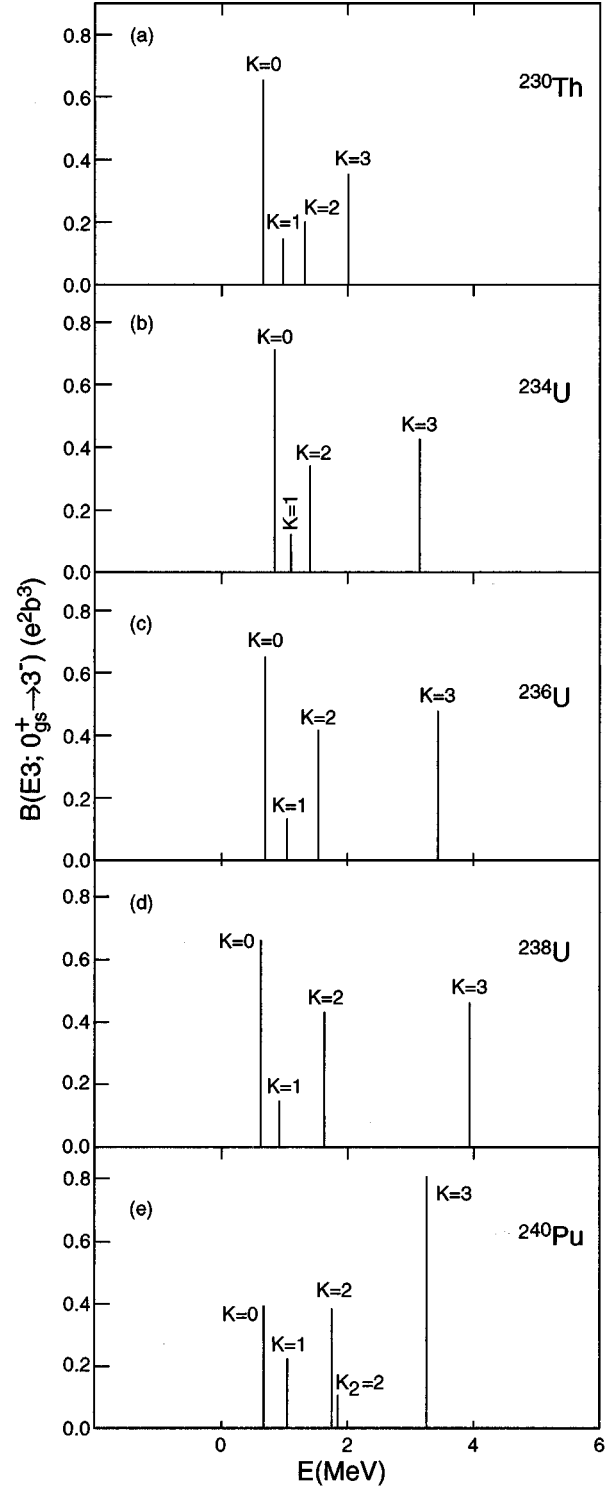


FIG. 15. Calculated  $E3$  strength distributions for the  $K^\pi = 0^-, 1^-, 2^-$ , and  $3^-$  octupole states for  $^{230}\text{Th}$ ,  $^{234}\text{U}$ ,  $^{236}\text{U}$ ,  $^{238}\text{U}$ , and  $^{240}\text{Pu}$  with  $e_3 = 0.19e b^{3/2}$ . The subscript 2 denotes a  $J^\pi=3^-$  state built on a  $\gamma$  vibration.

energy relative to the  $J^\pi=3^-$  members of the  $K^\pi=0^-, 1^-,$  and  $2^-$  bands built on the ground state according to the relation [4]

$$E(K) = E_0 + (2N - 2)(4 - K^2)A_2 / \sqrt{6}. \quad (13)$$

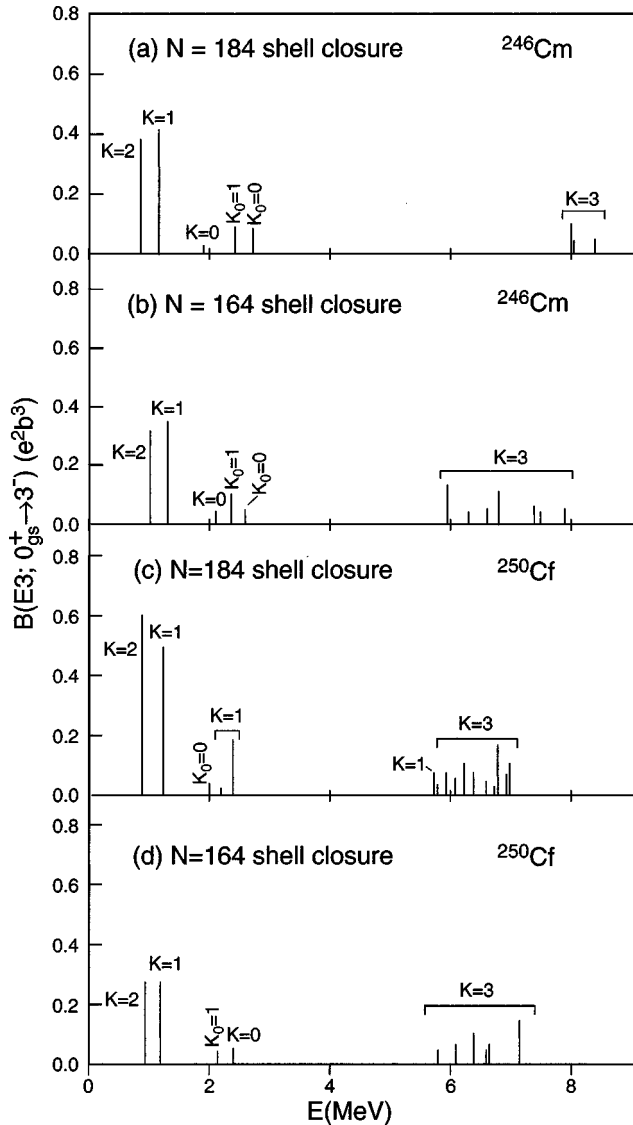


FIG. 16. Calculated  $E3$  strength distributions for the  $K^\pi=0^-$ ,  $1^-$ ,  $2^-$ , and  $3^-$  octupole states for  $^{246}\text{Cm}$  and  $^{250}\text{Cf}$ . Results assuming both the existence and nonexistence of the  $N=164$  subshell closure are shown. The subscript 0 denotes a  $J^\pi=3^-$  state built on a  $\beta$  vibration.

For a Hamiltonian corresponding to deformed nuclei but not in the  $SU(3)$  limit this pattern is altered, but the  $K^\pi=3^-$  state is still highest in energy. The effects of the quadrupole-quadrupole and exchange terms in the  $sd$ - $f$  interaction are explored in more detail in Ref. [5]. Here we simply present the results of the calculations of the distributions of  $E3$  strength from the ground state over a wide range of excitation energy for the nuclei under study (Figs. 15, 16). The effective charge was taken to be  $e_3=0.19 e b^{3/2}$ .

In all cases, the lowest-lying  $K^\pi=3^-$  state in the calculation is an octupole state built on the ground state. In  $^{230}\text{Th}$ ,  $^{234,236,238}\text{U}$ , and  $^{240}\text{Pu}$  (Fig. 15), the  $K^\pi=3^-$  strength is calculated to be concentrated in a single state at an energy between 2 and 4 MeV. In contrast, the  $K^\pi=3^-$  strength in  $^{246}\text{Cm}$  and  $^{250}\text{Cf}$  (Fig. 16) is calculated to be at much higher energies (near 8 MeV in  $^{246}\text{Cm}$  and 6 MeV in  $^{250}\text{Cf}$ ) and strongly fragmented. This fragmentation is not significantly changed if we consider the  $N=164$  subshell closure. The

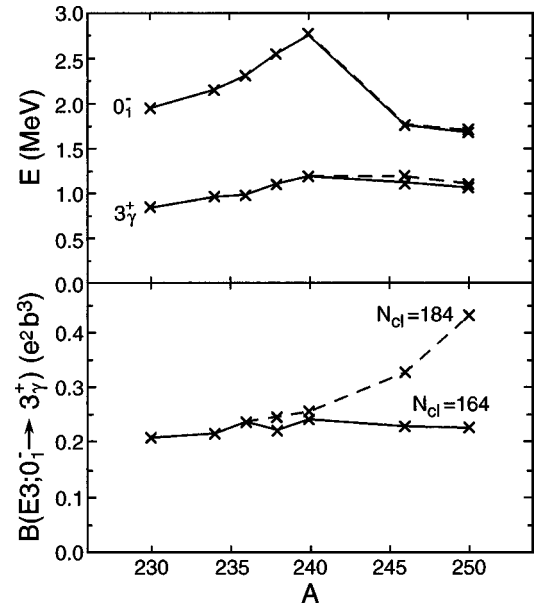


FIG. 17. Predicted values for the energies and  $B(E3; 0^- \rightarrow 3_g^+)$  values for the  $J^\pi=0^-$ ,  $K^\pi=0^-$  states resulting from the coupling of the  $J^\pi=3^+$  member of the  $\gamma$ -vibrational band with the  $J^\pi=3^-$  member of the  $K^\pi=2^-$  octupole band. Calculated values are indicated by crosses and the lines are included to guide the eye.

low-energy octupole resonance (LEOR), which is considered to be a  $1\hbar\omega$  excitation and is located near an energy of  $31A^{-1/3}$  MeV [6], would occur near 5 MeV in this mass region and would complicate an attempt to identify the  $K^\pi=3^-$  octupole strength in  $^{246}\text{Cm}$  and  $^{250}\text{Cf}$  and perhaps even the U and Pu isotopes, if the present predictions are valid. These predictions highlight the importance of further investigating the  $K^\pi=3^-$  strength in these nuclei.

## VII. MULTIPHONON STATES

Recently, there has been considerable discussion about the existence of multiphonon states in deformed nuclei. There is experimental and theoretical evidence for two-phonon octupole-quadrupole vibrational excitations in deformed nuclei [52], and the IBA includes such states [4]. When these states have  $J^\pi=3^-$ , the IBA predicts that they will sometimes have small but nonzero  $E3$  strength from the ground states. In Figs. 15, 16, these states are indicated by subscripts. The IBA also predicts the existence of a  $J^\pi=0^-$ ,  $K^\pi=0^-$  state resulting from the coupling of the  $J^\pi=3^+$  member of the  $\gamma$ -vibrational band with the  $J^\pi=3^-$  member of the  $K^\pi=2^-$  octupole band. Predictions for both the energies and  $B(E3; 0^- \rightarrow 3_g^+)$  values for these states are displayed in Fig. 17.

The version of the IBA-1 used in the present work cannot calculate two-octupole-phonon states because it includes only one  $f$  boson. However, the possible importance of two-octupole-phonon states in the structure of heavy deformed nuclei has already been argued [53], and studies of multiple- $f$ -boson states should be pursued.

The present results on both single-phonon and multiphonon states differ from those in a recent study of octupole states in some actinide nuclei (including several studied here) with the coherent state model (CSM) [54]. In the CSM,

it is assumed that the  $K^\pi=1^-$  bandhead is created by the coupling of an octupole phonon to the  $J^\pi=2^+$  state, and the  $K^\pi=2^-$  bandhead results from the coupling of an octupole phonon to the  $J^\pi=0^+$  state. The  $K^\pi=3^-$  octupole state is not addressed at all in the CSM. Further theoretical investigations of multiphonon states will be needed to thoroughly understand the nature of the lowest collective octupole states in deformed nuclei.

### VIII. SUMMARY

We have studied octupole states in even-even nuclei in the deformed actinide region using the IBA-1 with one  $f$  boson by adopting the extended consistent- $Q$  formalism [8] to describe the positive parity core and a prescription for setting the parameter  $\epsilon_f$  similar to that used for the deformed rare-earth region in Ref. [5]. To examine the possibility that a spherical subshell closure exists at  $N=164$  as suggested in Ref. [7], we performed two sets of calculations for each nucleus with  $N \geq 146$ —one assuming the existence of the subshell closure, and the other assuming only the major shell closure at  $N=184$ . We succeeded in reproducing the energies of the  $K^\pi=0^-, 1^-,$  and  $2^-$  bands, the general behavior

of many  $E1$  transitions and the distribution of  $E3$  strength for these bands, and we are able to achieve the latter with the adoption of single octupole effective charge for all seven nuclei studied. A comparison of the two calculations of the  $E3$  strength distribution in  $^{250}\text{Cf}$  (assuming  $N=164$  and  $184$  shell closures) with the data favors the existence of  $N=164$  gap. This conclusion is also supported by the anomalous values of the parameters required to reproduce the positive parity states in  $^{250}\text{Cf}$  without the  $N=164$  subshell closure. In addition, we predicted that  $K^\pi=3^-$  octupole states in  $^{246}\text{Cm}$  and  $^{250}\text{Cf}$  occur at energies of 6 MeV or above and are strongly fragmented. Finally, we have predicted energies and  $B(E3; 0^- \rightarrow 3^+_\gamma)$  values for the  $J^\pi=0^-, K^\pi=0^-$  states which result from the coupling of  $\gamma$ - and octupole-vibrational states.

### ACKNOWLEDGMENTS

We wish to thank R. F. Casten for his many helpful comments. The present work was supported by the National Science Foundation, the U.S. Department of Energy under Contract Nos. DE-FG02-91ER40609 and DE-FG02-88ER40417, and the State of Florida.

- 
- [1] K. Neergard and P. Vogel, Nucl. Phys. **A145**, 33 (1970).  
 [2] A. Arima and F. Iachello, Phys. Rev. Lett. **35**, 1069 (1975).  
 [3] A. Arima and F. Iachello, Ann. Phys. (N.Y.) **111**, 201 (1978).  
 [4] A. F. Barfield, B. R. Barrett, J. L. Wood, and O. Scholten, Ann. Phys. (N.Y.) **182**, 344 (1988).  
 [5] P. D. Cottle and N. V. Zamfir, Phys. Rev. C **54**, 176 (1996).  
 [6] M. W. Kirson, Phys. Lett. **108B**, 237 (1982).  
 [7] D. S. Brenner, N. V. Zamfir, and R. F. Casten, Phys. Rev. C **50**, 490 (1994).  
 [8] P. O. Lipas, P. Toivonen, and D. D. Warner, Phys. Lett. **155B**, 295 (1985).  
 [9] W. T. Chou, N. V. Zamfir, and R. F. Casten, Phys. Rev. C **56**, 829 (1997).  
 [10] R. C. Thompson, J. R. Huizenga, and Th. W. Elze, Phys. Rev. C **12**, 1227 (1975).  
 [11] Y. A. Akovali, Nucl. Data Sheets **69**, 155 (1993).  
 [12] P. C. Sood, D. M. Headly, and R. K. Sheline, At. Data Nucl. Data Tables **51**, 273 (1992).  
 [13] J. S. Boyno, J. R. Huizenga, Th. W. Elze, and C. E. Bemis, Jr., Nucl. Phys. **A209**, 125 (1973).  
 [14] Y. A. Akovali, Nucl. Data Sheets **71**, 181 (1994).  
 [15] M. R. Schmorak, Nucl. Data Sheets **63**, 183 (1991).  
 [16] F. K. McGowan and W. T. Milner, Nucl. Phys. **A571**, 569 (1994).  
 [17] E. N. Shurshikov, Nucl. Data Sheets **53**, 601 (1988).  
 [18] D. Ward, H. R. Andrews, G. C. Ball, A. Galindo-Uribarri, V. P. Janzen, T. Nakatsukasa, D. C. Radford, T. E. Drake, J. DeGraaf, S. Pilotte, and Y. R. Shimizu, Nucl. Phys. **A600**, 88 (1996).  
 [19] E. N. Shurshikov and N. V. Timofeeva, Nucl. Data Sheets **59**, 947 (1990).  
 [20] S. W. Yates, A. M. Friedman, and I. Ahmad, Phys. Rev. C **12**, 795 (1975).  
 [21] M. R. Schmorak, Nucl. Data Sheets **57**, 515 (1989).  
 [22] I. Ahmad, A. M. Friedman, and S. W. Yates, Phys. Rev. C **21**, 874 (1980).  
 [23] M. R. Schmorak, Nucl. Data Sheets **57**, 558 (1989).  
 [24] O. Scholten, Phys. Lett. **127B**, 144 (1983).  
 [25] J. Rikovska and D. Bonatsos, Phys. Lett. B **211**, 259 (1988).  
 [26] P. D. Cottle, K. A. Stuckey, and K. W. Kemper, Phys. Rev. C **38**, 2843 (1988).  
 [27] Th. W. Elze and J. R. Huizenga, Nucl. Phys. **A187**, 545 (1972).  
 [28] F. K. McGowan and W. T. Milner, Nucl. Phys. **A562**, 241 (1993).  
 [29] A. Bohr and B. R. Mottelson, *Nuclear Structure* (Benjamin, New York, 1975), Vol. II.  
 [30] P. D. Cottle and D. A. Bromley, Phys. Lett. B **182**, 129 (1986).  
 [31] N. V. Zamfir, R. F. Casten, and P. von Brentano, Phys. Lett. B **226**, 11 (1989).  
 [32] O. Scholten, The program package PHINT, Kernfysisch Versneller Instituut Internal Report No. 63, 1979.  
 [33] S. Bjornholm, J. Dubois, and B. Elbek, Nucl. Phys. **A118**, 241 (1968).  
 [34] P. Vogel, Phys. Lett. **60B**, 431 (1976).  
 [35] N. V. Zamfir, O. Scholten, and P. von Brentano, Z. Phys. A **337**, 293 (1990).  
 [36] B. Ackermann, H. Baltzer, K. Freitag, C. Günther, P. Herzog, J. Manns, U. Müller, R. Paulsen, P. Sevenich, T. Weber, B. Will, J. de Boer, G. Graw, A. I. Levon, M. Loewe, A. Löscher, and E. Müller-Zanotti, Z. Phys. A **350**, 13 (1994).  
 [37] P. von Brentano, N. V. Zamfir, and A. Zilges, Phys. Lett. B **278**, 221 (1992).  
 [38] A. Zilges, P. von Brentano, R.-D. Herzberg, U. Kneissl, J. Margraf, H. Maser, N. Pietralla, and H. H. Pitz, Phys. Rev. C **52**, R468 (1995).

- [39] C. M. Lederer, Phys. Rev. C **24**, 1175 (1981).
- [40] P. D. Cottle, Phys. Rev. C **47**, 1529 (1993).
- [41] G. A. Leander, W. Nazarewicz, G. F. Bertsch, and J. Dudek, Nucl. Phys. **A453**, 58 (1986).
- [42] R. J. Poynter, P. A. Butler, N. Clarkson, D. Cline, K. A. Connell, R. A. Cunnigham, L. Goettig, T. H. Hoare, J. R. Hughes, N. S. Jarvis, G. D. Jones, S. Juutinen, S. M. Mullins, C. N. Pass, J. Simpson, R. Wadsworth, D. L. Watson, and C. A. White, Phys. Lett. B **232**, 447 (1989).
- [43] H. Mach, W. Nazarewicz, D. Kusnezov, M. Moszynski, B. Fogelberg, M. Hellström, L. Spanier, R. L. Gill, R. F. Casten, and A. Wolf, Phys. Rev. C **41**, R2469 (1990).
- [44] D. W. S. Chan, J. J. Egan, A. Mittler, and E. Sheldon, Phys. Rev. C **26**, 841 (1982).
- [45] S. Bjornholm, J. Borggreen, D. Davies, N. J. S. Hansen, J. Pedersen, and H. L. Nielsen, Nucl. Phys. **A118**, 261 (1968).
- [46] C. Ardisson, J. Dalmaso, and G. Ardisson, Phys. Rev. C **33**, 2132 (1986).
- [47] K. Katori, A. M. Friedman, and J. R. Erskine, Phys. Rev. C **8**, 2336 (1973).
- [48] W. J. B. Winter, A. H. Wapstra, P. F. A. Goudsmit, and J. Konijn, Nucl. Phys. **A197**, 417 (1972).
- [49] P. P. Parekh, L. K. Peker, S. Katcoff, and E.-M. Franz, Phys. Rev. C **26**, 2178 (1982).
- [50] F. K. McGowan, C. E. Bemis, Jr., W. T. Milner, J. L. C. Ford, Jr., R. L. Robinson, and P. H. Stelson, Phys. Rev. C **10**, 1146 (1974).
- [51] F. Iachello and A. Arima, *The Interacting Boson Model* (Cambridge University Press, Cambridge, 1987).
- [52] U. Kneissl, A. Zilges, J. Margraf, I. Bauske, P. von Brentano, H. Friedrichs, R. D. Heil, R.-D. Herzberg, H. H. Pitz, B. Schlitt, and C. Wesselborg, Phys. Rev. Lett. **71**, 2180 (1993).
- [53] R. Piepenbring, Phys. Rev. C **27**, 2968 (1983).
- [54] A. A. Raduta, N. Lo Iudice, and I. I. Ursu, Nucl. Phys. **A608**, 11 (1996).